

Tailored electric and magnetic photonic local density of states of dielectric nanostructures revealed by rare-earth doped films

Peter R. Wiecha,^{1,*} Clément Majorel,¹ Christian Girard,¹ Arnaud Arbouet,¹ Bruno Masenelli,² Olivier Boisson,³ Aurélie Lecestre,⁴ Guilhem Larrieu,⁴ Vincent Paillard,¹ and Aurélien Cuche^{1,†}

¹*CEMES, Université de Toulouse, CNRS, Toulouse, France*

²*Université de Lyon, INSA-Lyon, ECL, UCBL, CPE, CNRS, INL-UMR5270, Villeurbanne, France*

³*Université de Lyon, CNRS, ILM-UMR 5306, Villeurbanne, France*

⁴*LAAS, Université de Toulouse, CNRS, INP, Toulouse, France*

We propose a simple experimental technique to separately map the electric and magnetic components of the photonic local density of states (LDOS) of single dielectric nanostructures, using a few nanometer thin film of rare-earth ion doped clusters. Rare-earth ions provide electric and magnetic dipole transitions of similar magnitude. By recording the photoluminescence from the deposited layer excited by a focused laser beam, we are able to simultaneously map the electric and magnetic LDOS of individual nanostructures. In spite of being a diffraction-limited far-field method with a spatial resolution of a few hundred nanometers, our approach appeals by its simplicity and high signal-to-noise ratio. We demonstrate our technique at the example of single silicon nanorods and dimers, in which we find a significant separation of electric and magnetic near-field contributions. Our method paves the way towards the efficient and rapid characterization of the electric and magnetic optical response of complex photonic nanostructures.

In the last decades, photonic nanostructures emerged as powerful instruments to control light at the subwavelength scale.¹ The interest in nano-optics lies usually in the control of the optical *electric* field, since the response of materials to rapidly oscillating magnetic fields is extremely weak. Actually, materials with a substantial magnetic response to electromagnetic radiation (*i.e.* $\mu \neq 1$) are not known in nature. However, properly designed nanostructures allow to significantly boost the magnetic response. For instance metallic (split-)ring resonators support a magnetic moment which is proportional to the area covered by the ring's aperture. For frequencies in the visible range this area is usually about 10^6 times larger than the equivalent area in atoms, defined by the Bohr radius, which explains the emergence of observable effects related to the optical magnetic field.² In consequence, it is possible to overcome the natural limitation to $\mu = 1$ by designing so-called meta-materials, which are ordered arrangements of meta-units like splitting resonators.³

Using metals requires nanostructures of complex shape to obtain a significant magnetic response. On the other hand, in dielectrics of high refractive index, a magnetic response arises naturally from the curl of the electric field.^{4,5} Very simple geometries like spheres⁶ or cylinders⁷ are actually sufficient to induce a strong magnetic field enhancement.⁸ An additional advantage of high-index dielectric nanostructures is their low dissipation. Silicon (Si) for example has a very low absorption through the entire visible range compared to noble metals.⁹ This weak absorption associated to the indirect gap in the near infrared becomes cumbersome only for applications involving propagation of visible light across distances of tens

to hundreds of microns. Thus, in small dielectric nanostructures the absorption can usually be neglected.¹⁰ In summary, high-index dielectric nanostructures seem to be an appropriate platform to study the confinement of optical electric and magnetic fields. Most importantly, it has been shown that the electric and magnetic fields are located in different regions around dielectric nanostructures. In other words, the electric and magnetic parts of the photonic local density of states (LDOS) can be spatially separated around subwavelength small particles.^{11,12}

The separation of magnetic and electric field energy close to photonic nano-structures was first demonstrated by measuring the local magnetic field intensity using scanning near-field optical microscopy (SNOM). The sensitivity to the magnetic part of the optical near-field is provided by particular SNOM-tips, coated with nanoscale metal rings or split-ring resonators.^{13–16} Another possibility to access the LDOS is to use optical quantum transitions as near-field probe and exploit the proportionality of the LDOS to the decay rate of a quantum emitter.^{17–20} However, in order to discriminate between electric and magnetic LDOS, probes supporting both electric and magnetic dipole transitions need to be used. This drastically limits the range of possible emitters: Electric dipole (ED) transitions are usually 4–5 orders of magnitude stronger than magnetic dipole (MD) transitions.²¹ Still, intense MD transitions can be found occasionally, for instance in lanthanoid ions (also known as rare earth elements), such as europium (Eu^{3+}),²² which have recently been suggested as probes for the detection of the optical magnetic field.^{23,24} A peculiarity of Eu^{3+} is that electric and magnetic dipole transitions of comparable strength occur at close wavelengths. Both start from the 5D_0 energy level via deexcitation to the 7F_2 (ED) and the 7F_1 level (MD).²⁵ Those transitions lie in the visible, around $\lambda_{\text{ED}} \approx 610 \text{ nm}$ and

* e-mail : peter.wiecha@cemes.fr

† e-mail : cuche@cemes.fr

$\lambda_{\text{MD}} \approx 590 \text{ nm}$.²³ This renders europium ions particularly promising as potential probes for the electric and magnetic LDOS around dielectric nanostructures: despite their similar transition energies, the ED and MD transitions are spectrally separated enough to easily distinguish them *e.g.* using simple color-filters.

Thanks to their unique properties, rare-earth ion doped media have been used as probes to determine the relative intensities of electric and magnetic LDOS at fixed positions or on non-structured samples like interfaces.^{26–28} By attaching an Eu^{3+} doped nano-crystal to a SNOM tip, the 3D spatial distribution of the electric and magnetic LDOS on top of gold strips has been recorded.¹⁸ The methods employed in these studies are either based on rare-earth emitters at fixed position,^{23,28} or require complex experimental setups (SNOM-type approach).^{18,29}

In this letter, we propose an alternative and complementary approach: we deposit a nanometric thin film of Eu^{3+} -doped nano-clusters on high-index dielectric nanostructures and raster-scan the sample under a tightly focused diffraction limited laser beam. In this configuration, the laser beam is taking the role of the SNOM-tip. In the following, we report experimental maps of the luminescence from either the electric or magnetic dipole transitions. These results show the good signal to noise ratio and spatial resolution obtained with a rather simple approach. We also compare our experimental results with computed maps of the electric and magnetic radiative LDOS.

I. PHOTOLUMINESCENCE FROM Eu^{3+} -DOPED NANOCLUSTER FILM DEPOSITED ON SILICON NANOSTRUCTURES

Sample preparation

Our sample contains single crystalline silicon dimers consisting of two elements, each $300 \times 300 \times 90 \text{ nm}^3$ ($L \times W \times H$) large, separated by a gap G of variable size. These nanostructures are fabricated in a top-down approach, where a single layer of negative-tone resist, namely hydrogen silsesquioxane (HSQ), is patterned by electron-beam lithography.³⁰ Subsequent reactive ion etching in the $H = 90 \text{ nm}$ Si overlayer of commercial silicon on insulator (SOI) substrates defines the structures. The remaining HSQ-layer on the top of the structures induces an additional SiO_2 capping of approximately 20 nm . This layer acts as a spacer between the nanostructures and the Eu^{3+} doped film. For more details on the fabrication process, see Ref. 31. After the lithography, a 30 nm thick film of Eu^{3+} -doped Gd_2O_3 nano-clusters is deposited. This thickness is a good trade-off between luminescence intensity from the emitters and planar homogeneity. The film is synthesized by the Low Energy Cluster Beam Deposition (LECBD) technique. LE CBD consists in the ablation of a solid Gd_2O_3 pellet, doped

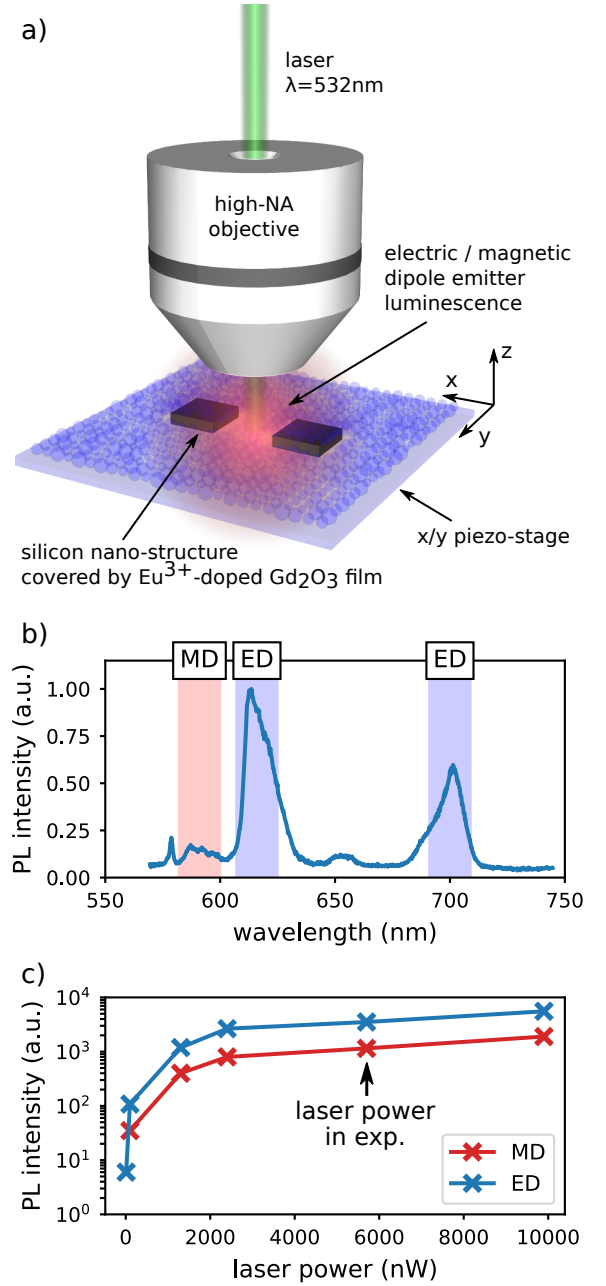


FIG. 1. a) Sketch of the experimental setup. A tightly focused laser beam ($\text{NA } 0.9$, $\lambda = 532 \text{ nm}$) is raster-scanned over a high-index dielectric nano-structure (in our case: silicon). An Eu^{3+} -doped Gd_2O_3 film is deposited on the structure. The photoluminescence due to the magnetic and electric dipole transitions of the europium ions is collected in back-scattering by the microscope objective and analyzed with a spectrometer at each raster-scan position. b) Example spectrum of the photoluminescence from the Eu^{3+} -ion. Emission due to magnetic dipole (MD) and electric dipole (ED) transitions are underlined by red and blue color, respectively. c) PL intensity as function of laser power. The power used for the acquisition of the maps was around 5700 nW .

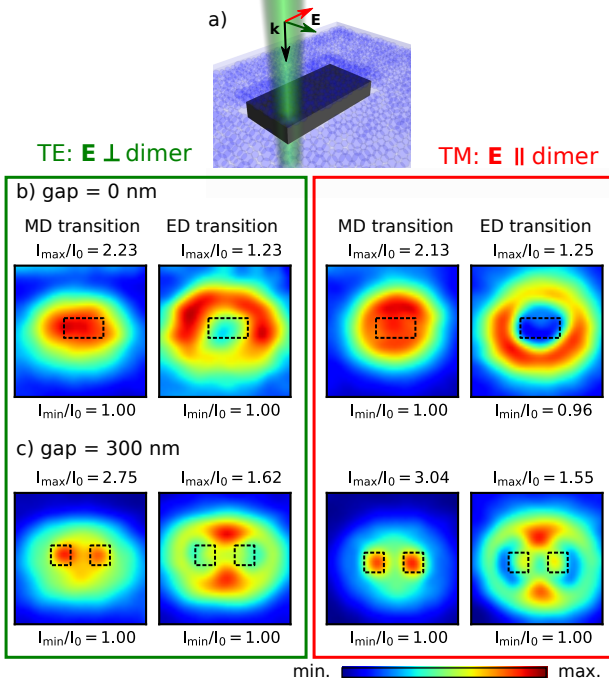


FIG. 2. Experimental mappings for different laser polarizations (sketch shown in a) for gap sizes of b) $G = 0$ nm and c) $G = 300$ nm. left: TE polarized laser (electric field perpendicular to dimer long axis) right: TM polarized laser (\mathbf{E} along dimer long axis)

at 7% with europium, *via* a pulsed Nd:YAG laser (10 ns pulse width). The chosen doping concentration results in a good compromise to preserve the stoichiometry of the sesquioxide matrix as well as a high luminescence of the Europium ions, without impairing the crystallographic and optical properties of the clusters.³² The ablated fragments are then broken into small clusters, first by the injection of He (20 mbar) as a buffer gas in the nucleation chamber and subsequently during its adiabatic expansion through a micrometer nozzle. The resulting nanocrystals are deposited on the dielectric nanostructures without further breaking (“soft landing”). More details about the process and the resulting nanocrystals can be found in Refs. 29 and 33.

Experimental configuration

Our experimental setup consists of an optical microscope equipped for spectroscopy with a confocal pinhole of 100 μm . A simplified sketch of the experiment is shown in figure 1a. A linearly polarized cw laser at $\lambda = 532$ nm is focused by a $\times 100$ air objective (NA = 0.9) on the sample, which lies on a XY piezo stage. The photoluminescence (PL) from the sample is collected by the same microscope objective. The PL is dispersed by a grating (300 grooves per mm) and detected by a CCD

camera (Andor iDus 401), with an integration time of $t_{\text{exposure}} = 2$ s. A typical spectrum and saturation curve from the Eu^{3+} -doped Gd_2O_3 film is shown in figure 1b-c. Finally, we obtain 2D PL maps by raster-scanning the sample under the laser with the piezo-stage. At each position, we acquire a spectrum and extract the emission intensities from the spectral ranges corresponding to magnetic or electric transitions ($\lambda = (590 \pm 10)$ nm, respectively $\lambda = (610 \pm 10)$ nm) during post-processing. The signal is normalized to the background PL intensity, recorded far from the nanostructures. We note that our approach yields a high signal-to-noise ratio, which can be qualitatively seen for example in the spectra (see Fig. 1b, and experimental maps in Figs. 2 and 3). Also the diffraction limited resolution of the technique can be improved using an oil immersion objective and further increased in a TERS-like setup, using the near-field enhancement at a plasmonic tip to excite very small volumes of the emitter-doped film.³⁴

Experimental results

Figure 2 shows raster-scan maps, measured on silicon dimers with gap-sizes of 0 nm and 300 nm, obtained with an incident laser polarization perpendicular to (TE) and along (TM) the dimer long axis (see also [supporting informations \(SI\)](#) for further results). In the experimental maps, a clear inversion of the contrast between emission from MD and ED transitions is observed for both polarizations. Interestingly, both, TE and TM, yield almost identical raster-scan images. Keeping in mind that the ED and MD transitions in Eu^{3+} are both populated by excitation of the $^5\text{D}_1$ level via the local *electric* field,²⁵ this is a surprising finding because in the vicinity of the nano-dimers, the spatial near-field distribution depends significantly on the laser polarization (see also SI). Furthermore, figure 1c shows that we use an excitation power close to a saturation plateau in the PL intensity of the bare Eu^{3+} film. Together with the PL-mappings which are independent of the laser polarization, we conclude that we excite the Eu^{3+} ions close to saturation. In this regime, the observed variations in the ED (resp. MD) photoluminescence maps are predominantly driven by the electric (resp. magnetic) radiative LDOS at the *emission* wavelength. This conclusion is in agreement with a recent study of the directional emission of Eu^{3+} ions, coupled to plasmonic nanostructures. In the latter, the most significant modification of the Eu^{3+} -PL is ascribed to the improved light out-coupling, whereas the plasmonic enhancement of the excitation has only a weak impact on the emission.³⁵

We systematically measured PL maps on silicon dimers with gap-sizes between 0 nm and 300 nm, which are shown in figure 3b. For these results, the laser polarization was arbitrarily chosen perpendicular to the long axis of the dimers. Sketches and scanning electron microscopy (SEM) images of the corresponding structures

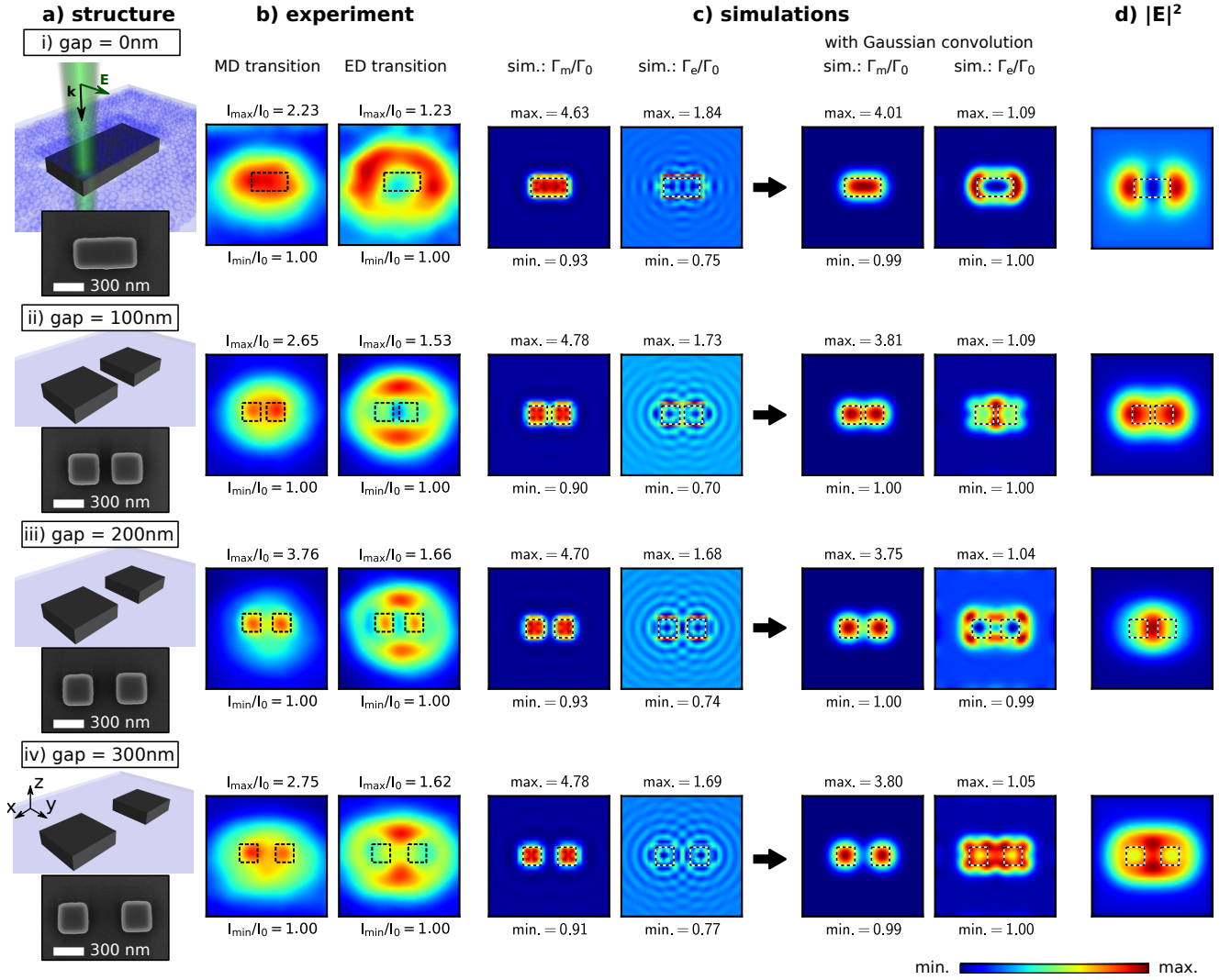


FIG. 3. Comparison of the experimental results with simulated decay-rate maps for different gap sizes i) $G = 0$ nm, ii) $G = 100$ nm, iii) $G = 200$ nm and iv) $G = 300$ nm. a) Sketches and SEM images of the corresponding structures. SEM images were taken prior to Eu^{3+} -cluster deposition. Scale bars are 300 nm. b) Experimental results recorded with an incident polarization along the dimer axis. Left column: MD transition, right column: ED transition. c) Simulated decay-rate maps before (left columns) and after convolution with a Gaussian profile (right columns). The subplots on the left show the magnetic dipole in-plane decay rates Γ_m^{xy} , the subplots on the right the respective ED maps Γ_e^{xy} . The waist of the Gaussian profile is $\eta = 200$ nm. All color-maps show areas of $2 \times 2 \mu\text{m}^2$, dashed lines indicate the positions of the silicon dimer. d) simulated maps of the average electric field intensity in the Eu^{3+} film as function of the spot position for a diffraction limited, TE polarized laser ($\lambda = 532$ nm, FWHM of 300 nm).

are shown in Fig. 3a. As already observed in figure 2, a clear inversion of the contrast between emission from MD and ED transitions is observed. The MD photoluminescence yields a maximum intensity when the laser-beam is focused on the structure. The ED emission maps on the other hand consistently contain valley-like features, where a reduction in intensity is surrounded by a stronger PL. A single nano-rod (figure 3i) yields one peak (MD) or one valley feature (ED). However, as soon as a gap is introduced (figures 3ii-iv), the maps start to change significantly. The magnetic dipole emission yields confined

hot-spots at the silicon block positions, whereas the PL maps from the ED transition show hot-spots outside the dimer, located above and below the gap. The ED maps show furthermore circular features around the two silicon blocks, each with a minimum PL intensity in the center.

We therefore infer, that the ED and MD maps recorded with our technique should reflect the electric, respectively magnetic radiative LDOS at the location of the Eu^{3+} -film. We will confirm this assumption in the following using numerical simulations.

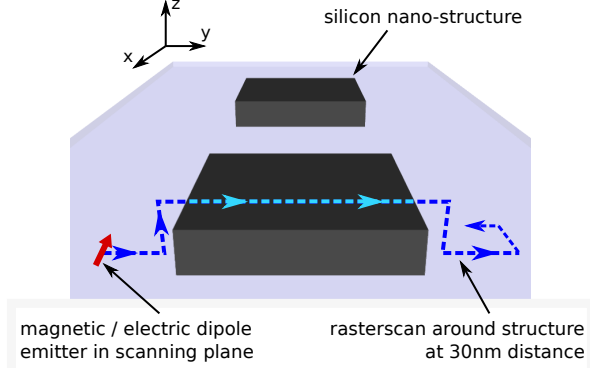


FIG. 4. Sketch of the simulation procedure. A magnetic or electric dipolar emitter is raster-scanned across the nano-structure at 30 nm above its surface, simulating the distance of the doped film to the top surface of the structures (20 nm SiO₂ spacing layer). Far from the structure, the scan-height is at 30 nm above the ground-level. The raster-scan is repeated for emitter orientations along 0X and 0Y, the decay-rates are averaged.

II. CALCULATING THE ELECTRIC AND MAGNETIC RADIATIVE LDOS

To confirm that our technique allows the simultaneous recording of the electric and magnetic radiative LDOS, we compare the experimental data to calculated LDOS maps.

Decay-rate of electric/magnetic emitters

The decay-rate enhancement of a quantum emitter is proportional to the partial LDOS at the emitter's location.^{19,36} With “partial” LDOS, we refer to the projection of the LDOS onto a specific direction (dipole orientation) and to the nature of the dipole transition (electric or magnetic). The full LDOS can be obtained by averaging over all possible dipole orientations. Hence, the computation of the decay-rate modification of electric and magnetic dipole transitions also yields the photonic local density of states.

The decay-rate of electric or magnetic dipolar transitions is modified by the presence of a polarizable material. The effect is intuitively understandable for an electric dipole transition \mathbf{p} , as a result of the enhancement (or weakening) of the electric near-field due to the dielectric contrast or optical resonances, and the back-action of the radiated field on the dipole emitter. It is possible to derive an integral equation describing the decay-rate Γ_e of an electric dipole transition at a position \mathbf{r}_0 , close

to an arbitrary nano-structure:^{12,19}

$$\Gamma_e(\mathbf{r}_0, \omega) = \Gamma_e^0(\omega) \times \left(1 + \frac{3}{2k_0^3} \mathbf{u} \cdot \text{Im}(\mathcal{S}_p^{\text{EE}}(\mathbf{r}_0, \mathbf{r}_0, \omega)) \cdot \mathbf{u} \right), \quad (1)$$

In this equation, $\Gamma_e^0(\omega) = 4k_0^3 p^2 / 3\hbar$ is the decay rate of the emitter in the absence of a structure with the vacuum wavenumber k_0 . \mathbf{u} and p denote the dipole orientation and amplitude, respectively, and

$$\mathcal{S}_p^{\text{EE}}(\mathbf{r}, \mathbf{r}_0, \omega) = \int_V d\mathbf{r}' \int_V d\mathbf{r}'' \chi(\mathbf{r}', \omega) \mathbf{G}^{\text{EE}}(\mathbf{r}, \mathbf{r}', \omega) \cdot \mathbf{K}(\mathbf{r}', \mathbf{r}'', \omega) \cdot \mathbf{G}^{\text{EE}}(\mathbf{r}'', \mathbf{r}_0, \omega). \quad (2)$$

\mathbf{K} is the generalized propagator (see *e.g.* Ref. 37). The propagator \mathbf{G}^{EE} can be found by identification using the electric field emitted by a dipolar source³⁸ and the Green's Dyad for vacuum³⁷ (*c.f.* also Ref. 12).

Eq. (1) describes the decay-rate of an *electric* quantum emitter. It turns out, that although no known material has a direct response to rapidly oscillating magnetic fields, the decay rate of a magnetic dipole transition is nevertheless influenced by the presence of material. Such *magnetic-magnetic* response function associated with a structure which, by itself, has no direct magnetic response, arises from the *electric* field emitted by the magnetic dipole, which can interact with the environment. In particular, Mie-type optical resonances in dielectric nanostructures often induce curled features in the electric near-field spatial distribution, leading to a strong enhancement of the magnetic field via the Maxwell's equation $ik_0 \mathbf{B}(\mathbf{r}) = \text{rot} \mathbf{E}(\mathbf{r})$ (for monochromatic fields, $k_0 = 2\pi/\lambda_0$). Formally, the magnetic decay-rate in the vicinity of arbitrary nanostructures can be calculated in complete analogy to equation (1) by replacing the tensors \mathbf{G}^{EE} in equation (2) with the Dyads \mathbf{G}^{HE} (first occurrence) and \mathbf{G}^{EH} (second occurrence, *c.f.* reference 12). The latter tensors are often called “mixed-field susceptibilities”.^{39–41}

Simulation of raster-scan maps

To solve Eq. (1) numerically, the integrals in Eq. (2) can be converted to discrete sums over the mesh-points of a volume-discretized nanostructure. To calculate raster-scans of the MD and ED decay-rates (hence maps of the electric and magnetic LDOS), we make use of the concept of a generalized propagator.³⁷ This approach significantly speeds up the computation of the decay-rate at multiple locations, as explained in reference 42.

The specific simulation procedure is illustrated in figure 4. We raster-scan a dipolar emitter of either magnetic (Γ_m , $\lambda_{\text{MD}} = 590$ nm) or electric nature (Γ_e , $\lambda_{\text{ED}} = 610$ nm) across a discretized nano-dimer (discretization step $s = 20$ nm). The dimer lies in a homogeneous environment of refractive index $n_{\text{env}} = 1.8$, corresponding to

the optical index of the Gd_2O_3 film.⁴³ For an analysis of the impact of the environment refractive index, [see also SI](#). The distance between emitter and structure is kept at 30 nm. Far from the structure, the dipole is scanned at 30 nm above the substrate. In this way, we account for the distance between the Eu^{3+} -cluster film and the nanostructures due to the 20 nm thick SiO_2 layer (for an analysis of the emitter-structure distance, [see SI](#)). We neglect dipole emitters oriented along OZ , because their emission, a toroidal radiation pattern propagating perpendicular to the Z -axis, is not detected in our experimental configuration ([see also SI](#)). Therefore, the simulated maps only take into account dipoles located in a plane parallel to the substrate (the computed values being the average of the contributions of dipoles oriented along OX and OY). We denote these average decay rates Γ_m^{xy} and Γ_e^{xy} for MD and ED, respectively.

The direct result of this procedure has a far too high spatial resolution (see the two columns on the left of figure 3c). Therefore, to account for the diffraction limited size of the laser-spot, and hence the excitation of a whole ensemble of emitters, we convolve the simulated mapping with a Gaussian profile of waist $\eta = 200$ nm (corresponding to a full width at half maximum of around 450 nm which is an upper estimate for the emission area.^{44,45} (See also [supporting informations](#) for a comparison of different convolutional sizes).

Our numerical signal power is described by the following equation:

$$I_{\text{signal}}(\mathbf{r}) = \int_{A_{\text{spot}}} \hbar\omega_0 n(\mathbf{r}') \Gamma_i^{xy}(\mathbf{r}') \exp\left(-\frac{\mathbf{r}'^2}{2\eta^2}\right) d\mathbf{r}'. \quad (3)$$

The integral runs over the area of the laser-spot A_{spot} , $\hbar\omega_0$ is the photon energy of the MD or ED transition, n is the density of emitting Eu^{3+} ions (which we consider homogeneous). Γ_i^{xy} is the x - y -averaged decay rate of either a magnetic ($i = "m"$) or an electric ($i = "e"$) dipole transition. The exponential factor accounts for the Gaussian intensity profile of the laser beam. The simulated maps after convolution are shown in the right columns of Fig. 3c. We note that a similar procedure has been successfully used to recover the near-field intensity distribution from two-photon luminescence (TPL) measurements on plasmonic nanostructures.⁴⁶

Discussion

Comparing the simulated and experimental results in figure 3, we observe that the features in the simulated maps are more confined around the dimer blocks. Nevertheless there is a general qualitative agreement. The global features and trends observed in the experimental maps are reproduced by the simulations. The contrasts of electric and/or magnetic LDOS close to dielectric nanostructures are in agreement with recently published experimental results, showing a clear separation of electric

and magnetic LDOS above the dielectric structures.^{24,47} Also the quantitative trends in the intensity ratios are correctly recovered by the simulations, showing an enhancement of the luminescence intensity by a factor of around 3 for the MD transition and 1.5 in the ED case.

Compared to the simulations, the experimental results are less sharp and possess broader features. Several effects can contribute to this broadening, first of all, we are not entirely at saturation, which can be seen in figure 1c, and the laser spot is of finite, diffraction limited size, hence excites a large collection of emitters at each raster-scan position. Those at the edge of the laser focal spot are excited with a weaker field amplitude, hence not at saturation. In the LDOS simulations on the other hand, we only take into account a single, saturated point-emitter, raster-scanned across the silicon dimer. Therefore, a residual contribution of the excitation electric field at the laser wavelength cannot be totally neglected. To elucidate this effect, we calculate the average electric near-field intensity in the Eu^{3+} doped film at each laser-spot position, shown in figure 3d for TE polarization (see also the [SI](#) for the TM case). The excitation is at $\lambda = 532$ nm with a spot size of 300 nm FWHM, corresponding to our experiment. There seem to be a certain resemblance between electric LDOS and excitation field pattern, which makes sense, because the near-field is correlated to the LDOS, even though we compare LDOS and $|\mathbf{E}|^2$ at different wavelengths. The magnetic part of the LDOS on the other hand does not show comparable features. This clear contrast confirms, that the experimental mappings are mainly driven by the electric and magnetic LDOS, while a certain broadening can be explained by a residual contribution of the excitation electric field of the laser. In addition, light might be guided through the dimer when the laser hits one extremity, and Europium ions at the other end, far from the laser spot can be remotely excited in this case as well. Such effect can result in a significant broadening of the spatial features in our mappings,^{44,45} and is not fully taken into account in our current theoretical model, even if an enlarged emission area is considered via the Gaussian convolution.

A better agreement could probably be achieved by simulating an actual “layer” of dipoles, instead of raster-scanning a single emitter, and by taking into account the modified radiation pattern due to the inhomogeneous environment.⁴⁸ However, this would require to consider the excitation intensity as function of the emitter position with respect to the center of the focal spot. A possible approach to the problem of non-saturated emitters could be the description of the Eu^{3+} emitters in the layer as three-level molecules.^{49,50} These more sophisticated theoretical approaches lie outside the scope of this study and will be the subject of a future work.

III. CONCLUSION

In conclusion, we demonstrated that the magnetic and electric LDOS can be tailored in the near-field of dielectric nanostructures. We obtained our results with a technique which allows the parallel mapping of the electric and magnetic components of the radiative LDOS via a far-field detection scheme. To this end, a nanometer thin film of rare-earth ion doped clusters is deposited on top of the structures and excited by a tightly focused laser beam. The laser beam is raster-scanned across the structures to obtain 2D maps of the LDOS. The emission from either electric or magnetic dipole transitions is extracted from the photoluminescence measurements, yielding the corresponding contributions to the local density of photonic states. Numerical simulations of the electric and magnetic LDOS show a general qualitative agreement with the experimental results and provide a good understanding of the underlying physical effects. These results show that the electric and magnetic near-field intensity

is confined in distinct regions around simple dielectric nanostructures such as rods or dimers. Our work paves the way towards the very rapid and simple experimental characterization of the response of photonic nanostructures to both, the electric and magnetic field of visible light and towards the tailoring of “on demand” magnetic and electric near-field landscapes of dielectric nanostructures.

ACKNOWLEDGMENTS

This work was supported by Programme Investissements d’Avenir under the program ANR-11-IDEX-0002-02, reference ANR-10-LABX-0037-NEXT, by the LAAS-CNRS micro and nanotechnologies platform, a member of the French RENATECH network and by the computing facility center CALMIP of the University of Toulouse under grant P12167.

-
- ¹ Lukas Novotny and Bert Hecht, *Principles of Nano-Optics* (Cambridge University Press, Cambridge ; New York, 2006).
 - ² Harald Giessen and Ralf Vogelgesang, “Glimpsing the Weak Magnetic Field of Light,” *Science* **326**, 529–530 (2009).
 - ³ J. B. Pendry, “Negative Refraction Makes a Perfect Lens,” *Physical Review Letters* **85**, 3966–3969 (2000).
 - ⁴ Roberto Merlin, “Metamaterials and the Landau–Lifshitz permeability argument: Large permittivity begets high-frequency magnetism,” *Proceedings of the National Academy of Sciences* **106**, 1693–1698 (2009).
 - ⁵ Arseniy I. Kuznetsov, Andrey E. Miroshnichenko, Yuan Hsing Fu, JingBo Zhang, and Boris Luk’yanchuk, “Magnetic light,” *Scientific Reports* **2**, 492 (2012).
 - ⁶ Andrey B. Evlyukhin, Sergey M. Novikov, Urs Zywi-etz, René Lyng Eriksen, Carsten Reinhardt, Sergey I. Bozhevolnyi, and Boris N. Chichkov, “Demonstration of Magnetic Dipole Resonances of Dielectric Nanospheres in the Visible Region,” *Nano Letters* **12**, 3749–3755 (2012).
 - ⁷ Polina Kapitanova, Vladimir Ternovski, Andrey Miroshnichenko, Nikita Pavlov, Pavel Belov, Yuri Kivshar, and Michael Tribelsky, “Giant field enhancement in high-index dielectric subwavelength particles,” *Scientific Reports* **7**, 731 (2017).
 - ⁸ Arseniy I. Kuznetsov, Andrey E. Miroshnichenko, Mark L. Brongersma, Yuri S. Kivshar, and Boris Luk’yanchuk, “Optically resonant dielectric nanostructures,” *Science* **354** (2016), 10.1126/science.aag2472.
 - ⁹ Pablo Albella, Rodrigo Alcaraz de la Osa, Fernando Moreno, and Stefan A. Maier, “Electric and Magnetic Field Enhancement with Ultralow Heat Radiation Dielectric Nanoantennas: Considerations for Surface-Enhanced Spectroscopies,” *ACS Photonics* **1**, 524–529 (2014).
 - ¹⁰ Pablo Albella, M. Ameen Poyli, Mikolaj K. Schmidt, Stefan A. Maier, Fernando Moreno, Juan José Sáenz, and Javier Aizpurua, “Low-Loss Electric and Magnetic Field-Enhanced Spectroscopy with Subwavelength Silicon Dimers,” *The Journal of Physical Chemistry C* **117**, 13573–13584 (2013).
 - ¹¹ Brice Rolly, Betina Bebey, Sebastien Bidault, Brian Stout, and Nicolas Bonod, “Promoting magnetic dipolar transition in trivalent lanthanide ions with lossless Mie resonances,” *Physical Review B* **85**, 245432 (2012).
 - ¹² Peter R. Wiecha, Arnaud Arbouet, Aurélien Cuche, Vincent Paillard, and Christian Girard, “Decay rate of magnetic dipoles near nonmagnetic nanostructures,” *Physical Review B* **97**, 085411 (2018).
 - ¹³ Eloïse Devaux, Alain Dereux, Eric Bourillot, Jean-Claude Weeber, Yvon Lacroute, Jean-Pierre Goudonnet, and Christian Girard, “Detection of the optical magnetic field by circular symmetry plasmons,” *Applied Surface Science* **164**, 124–130 (2000).
 - ¹⁴ Eloïse Devaux, Alain Dereux, Eric Bourillot, Jean-Claude Weeber, Yvon Lacroute, Jean-Pierre Goudonnet, and Christian Girard, “Local detection of the optical magnetic field in the near zone of dielectric samples,” *Physical Review B* **62**, 10504–10514 (2000).
 - ¹⁵ M. Buresi, D. van Oosten, T. Kampfrath, H. Schoenmaker, R. Heideman, A. Leinse, and L. Kuipers, “Probing the Magnetic Field of Light at Optical Frequencies,” *Science* **326**, 550–553 (2009).
 - ¹⁶ I. V. Kabakova, A. de Hoogh, R. E. C. van der Wel, M. Wulf, B. le Feber, and L. Kuipers, “Imaging of electric and magnetic fields near plasmonic nanowires,” *Scientific Reports* **6** (2016), 10.1038/srep22665.
 - ¹⁷ Ch Girard, T David, C Chicanne, A Mary, G. Colas des Francs, E Bourillot, J.-C Weeber, and A Dereux, “Imaging surface photonic states with a circularly polarized tip,” *Europhysics Letters (EPL)* **68**, 797–803 (2004).
 - ¹⁸ L. Aigouy, A. Cazé, P. Gredin, M. Mortier, and R. Carmi-nati, “Mapping and Quantifying Electric and Magnetic Dipole Luminescence at the Nanoscale,” *Physical Review Letters* **113**, 076101 (2014).

- ¹⁹ R. Carminati, A. Cazé, D. Cao, F. Peragut, V. Krachmalnicoff, R. Pierrat, and Y. De Wilde, “Electromagnetic density of states in complex plasmonic systems,” *Surface Science Reports* **70**, 1–41 (2015).
- ²⁰ A. Cuche, M. Berthel, U. Kumar, G. Colas des Francs, S. Huant, E. Dujardin, C. Girard, and A. Drezet, “Near-field hyperspectral quantum probing of multimodal plasmonic resonators,” *Physical Review B* **95**, 121402 (2017).
- ²¹ Tim H. Taminiau, Sinan Karaveli, Niek F. van Hulst, and Rashid Zia, “Quantifying the magnetic nature of light emission,” *Nature Communications* **3**, ncomms1984 (2012).
- ²² W. T. Carnall, P. R. Fields, and K. Rajnak, “Spectral Intensities of the Trivalent Lanthanides and Actinides in Solution. II. Pm^{3+} , Sm^{3+} , Eu^{3+} , Gd^{3+} , Tb^{3+} , Dy^{3+} , and Ho^{3+} ,” *The Journal of Chemical Physics* **49**, 4412–4423 (1968).
- ²³ N. Noginova, G. Zhu, M. Mavy, and M. A. Noginov, “Magnetic dipole based systems for probing optical magnetism,” *Journal of Applied Physics* **103**, 07E901 (2008).
- ²⁴ Maria Sanz-Paz, Cyrene Erandes, Juan Uriel Esparza, Geoffrey W. Burr, Niek F. van Hulst, Agnès Maitre, Lionel Aigouy, Thierry Gacoin, Nicolas Bonod, Maria F. Garcia-Parajo, Sébastien Bidault, and Mathieu Mivelle, “Enhancing Magnetic Light Emission with All-Dielectric Optical Nanoantennas,” *Nano Letters* (2018), 10.1021/acs.nanolett.8b00548.
- ²⁵ Denis G. Baranov, Roman S. Savelev, Sergey V. Li, Alexander E. Krasnok, and Andrea Alù, “Modifying magnetic dipole spontaneous emission with nanophotonic structures,” *Laser & Photonics Reviews* **11**, 1600268–n/a (2017).
- ²⁶ Sinan Karaveli and Rashid Zia, “Spectral Tuning by Selective Enhancement of Electric and Magnetic Dipole Emission,” *Physical Review Letters* **106**, 193004 (2011).
- ²⁷ R. Hussain, D. Keene, N. Noginova, and M. Durach, “Spontaneous emission of electric and magnetic dipoles in the vicinity of thin and thick metal,” *Optics Express* **22**, 7744–7755 (2014).
- ²⁸ Bongseok Choi, Masanobu Iwanaga, Yoshimasa Sugimoto, Kazuaki Sakoda, and Hideki T. Miyazaki, “Selective Plasmonic Enhancement of Electric- and Magnetic-Dipole Radiations of Er Ions,” *Nano Letters* **16**, 5191–5196 (2016).
- ²⁹ A. Cuche, B. Masenelli, G. Ledoux, D. Amans, C. Dujardin, Y. Sonnefraud, P. Mélinon, and S. Huant, “Fluorescent oxide nanoparticles adapted to active tips for near-field optics,” *Nanotechnology* **20**, 015603 (2009).
- ³⁰ Y. Guerfi, F. Carcenac, and G. Larrieu, “High resolution HSQ nanopillar arrays with low energy electron beam lithography,” *Microelectronic Engineering* **110**, 173–176 (2013).
- ³¹ Peter R. Wiecha, Arnaud Arbouet, Christian Girard, Aurélie Lecestre, Guilhem Larrieu, and Vincent Paillard, “Evolutionary multi-objective optimization of colour pixels based on dielectric nanoantennas,” *Nature Nanotechnology* **12**, 163–169 (2017).
- ³² B. Masenelli, G. Ledoux, D. Amans, C. Dujardin, and P. Mélinon, “Shells of crystal field symmetries evidenced in oxide nano-crystals,” *Nanotechnology* **23**, 305706 (2012).
- ³³ A. Perez, P. Melinon, V. Dupuis, L. Bardotti, B. Masenelli, F. Tournus, B. Prevel, J. Tuaillon-Combes, E. Bernstein, A. Tamion, N. Blanc, D. Tainoff, O. Boisson, G. Guiraud, M. Broyer, M. Pellarin, N. Fatti, F. Vallee, E. Cottancin, J. Lerme, J.-L. Vialle, C. Bonnet, P. Maioli, A. Crut, C. Clavier, J.-L. Rousset, and F. Morfin, “Functional nanostructures from clusters,” *International Journal of Nanotechnology* **7**, 523–574 (2010).
- ³⁴ C. Huang, A. Bouhelier, G. Colas des Francs, G. Legay, J.-C. Weeber, and A. Dereux, “Far-field imaging of the electromagnetic local density of optical states,” *Optics Letters* **33**, 300–302 (2008).
- ³⁵ S. Murai, M. Saito, H. Sakamoto, M. Yamamoto, R. Kamakura, T. Nakanishi, K. Fujita, M. A. Verschuuren, Y. Hasegawa, and K. Tanaka, “Directional outcoupling of photoluminescence from Eu(III) -complex thin films by plasmonic array,” *APL Photonics* **2**, 026104 (2017).
- ³⁶ Per Lunnemann and A. Femius Koenderink, “The local density of optical states of a metasurface,” *Scientific Reports* **6**, srep20655 (2016).
- ³⁷ Olivier J. F. Martin, Christian Girard, and Alain Dereux, “Generalized Field Propagator for Electromagnetic Scattering and Light Confinement,” *Physical Review Letters* **74**, 526–529 (1995).
- ³⁸ G. S. Agarwal, “Quantum electrodynamics in the presence of dielectrics and conductors. I. Electromagnetic-field response functions and black-body fluctuations in finite geometries,” *Physical Review A* **11**, 230–242 (1975).
- ³⁹ Christian Girard, Jean-Claude Weeber, Alain Dereux, Olivier J. F. Martin, and Jean-Pierre Goudonnet, “Optical magnetic near-field intensities around nanometer-scale surface structures,” *Physical Review B* **55**, 16487–16497 (1997).
- ⁴⁰ U. Schröter, “Modelling of magnetic effects in near-field optics,” *The European Physical Journal B* **33**, 297–310 (2003).
- ⁴¹ Ivana Sersic, Christelle Tuambilangana, Tobias Kampfrath, and A. Femius Koenderink, “Magnetolectric point scattering theory for metamaterial scatterers,” *Physical Review B* **83**, 245102 (2011).
- ⁴² Alexandre Teulle, Renaud Marty, Sviatlana Viarbitskaya, Arnaud Arbouet, Erik Dujardin, Christian Girard, and Gérard Colas des Francs, “Scanning optical microscopy modeling in nanoplasmonics,” *Journal of the Optical Society of America B* **29**, 2431 (2012).
- ⁴³ A. A. Dakhel, “Optical constants of evaporated gadolinium oxide,” *Journal of Optics A: Pure and Applied Optics* **3**, 452 (2001).
- ⁴⁴ Esther Wertz, Benjamin P. Isaacoff, Jessica D. Flynn, and Julie S. Biteen, “Single-Molecule Super-Resolution Microscopy Reveals How Light Couples to a Plasmonic Nanoantenna on the Nanometer Scale,” *Nano Letters* **15**, 2662–2670 (2015).
- ⁴⁵ David L. Mack, Emiliano Cortés, Vincenzo Giannini, Peter Török, Tyler Roschuk, and Stefan A. Maier, “Decoupling absorption and emission processes in super-resolution localization of emitters in a plasmonic hotspot,” *Nature Communications* **8**, 14513 (2017).
- ⁴⁶ Petru Ghenuche, Sudhir Cherukulappurath, Tim H. Taminiau, Niek F. van Hulst, and Romain Quidant, “Spectroscopic Mode Mapping of Resonant Plasmon Nanoantennas,” *Physical Review Letters* **101**, 116805 (2008).
- ⁴⁷ S. V. Makarov, I. S. Sinev, V. A. Milichko, F. E. Komissarenko, D. A. Zuev, E. V. Ushakova, I. S. Mukhin, Y. F. Yu, A. I. Kuznetsov, P. A. Belov, I. V. Iorsh, A. N. Podubny, A. K. Samusev, and Yu. S. Kivshar, “Nanoscale Generation of White Light for Ultrabroadband Nanospectroscopy,” *Nano Letters* **18**, 535–539 (2018).
- ⁴⁸ Alberto G. Curto, Tim H. Taminiau, Giorgio Volpe, Mark P. Kreuzer, Romain Quidant, and Niek F. van Hulst,

- “Multipolar radiation of quantum emitters with nanowire optical antennas,” [Nature Communications](#) **4**, 1750 (2013).
- ⁴⁹ Christian Girard, Olivier J. F. Martin, Gaëtan Lévêque, Gérard Colas des Francs, and Alain Dereux, “Generalized bloch equations for optical interactions in confined geometries,” [Chemical Physics Letters](#) **404**, 44–48 (2005).
- ⁵⁰ Gérard Colas des Francs, Christian Girard, Thierry Laroche, Gaëtan Lévêque, and Olivier J. F. Martin, “Theory of molecular excitation and relaxation near a plasmonic device,” [The Journal of Chemical Physics](#) **127**, 034701 (2007).